Evaluation of the Rayleigh-Gans approximation for microwave scattering by rimed snowflakes

Article

Accepted Version

Evaluation of the Rayleigh–Gans Approximation for Microwave Scattering by Rimed Snowflakes

Jussi Leinonen[a,b*], Stefan Kneifel[c], Robin J. Hogan[d,e]

[a] *Joint Institute for Regional Earth System Science and Engineering, University of California, Los Angeles, California, USA*
[b] *Jet Propulsion Laboratory, California Institute of Technology, Pasadena, California, USA*
[c] *Institute for Geophysics and Meteorology, University of Cologne, Cologne, Germany*
[d] *European Centre for Medium-Range Weather Forecasts, Reading, UK*
[e] *Department of Meteorology, University of Reading, Reading, UK*

[*]Correspondence to: Jussi Leinonen, MS 233-300, Jet Propulsion Laboratory, California Institute of Technology, Pasadena, CA 91109, USA. E-mail: jussi.s.leinonen@jpl.nasa.gov

We have evaluated of the applicability of the Rayleigh–Gans (RGA) and Self-Similar Rayleigh–Gans (SSRGA) approximations for microwave scattering by rimed snowflakes. This study extends previous findings that showed that, for unrimed snowflakes, the RGA is in good agreement with the discrete dipole approximation (DDA), which we used as a reference method. When riming is introduced, the RGA-derived scattering properties of individual snowflakes deviate significantly — up to 20–25 dB for the backscattering cross section at the W-band — from the corresponding DDA results. In contrast, the *average* scattering properties given by RGA are in good agreement with DDA for all but the most heavily rimed snowflakes: the mean bias in the backscattering cross section rarely exceeds 1 dB for light and moderate riming. We also found that an adjustment that accounts for the nonspherical shapes of the ice crystals can help eliminate a small constant bias found in RGA in earlier studies. The SSRGA approximates the RGA results with good accuracy at all degrees of riming, indicating that it, too, can be used with up to moderately rimed snowflakes.

Key Words: Rayleigh—Gans approximation; discrete dipole approximation; snowflakes; aggregation; riming; radar

Received . . .

1. Introduction

Global mapping and accurate characterization of snowfall is highly desirable for better constraining the energy budget and the hydrological cycle of the Earth. Its assimilation into numerical weather prediction models would also lead to improved forecasts, especially in high latitude regions where snowfall is the main precipitation type on the ground. Additionally, in mid-latitudes ice and snow particles play an important role inside clouds (Field and Heymsfield 2015). Recent studies found that over mid-latitude oceans and continents the vast majority of rainfall is generated via the ice phase (Mülmenstädt *et al.* 2015).

The challenges of remotely characterizing snow using microwave instruments stem from the complexity of natural frozen hydrometeors. The variety of particle shapes, sizes, densities, and orientations lead to complicated interactions with microwave radiation with wavelengths close to the size range of the particles. Therefore, in order to retrieve quantities like snow water content or particle size parameters, one must understand the relationship between scattering properties and parameters like the mass, size and structure of the snowflakes.

Several numerical methods, such as the discrete dipole approximation (DDA, Flatau and Draine 1994), can compute scattering properties accurately for arbitrarily shaped particles, but these methods are computationally demanding. Moreover, such methods are, by necessity, mathematically complex, which makes it difficult to analyze the correspondence between microphysical and scattering properties. Yet it is apparently critical to take the complex shape into account: several studies (Ishimoto 2008; Petty and Huang 2010; Tyynelä *et al.* 2011, among others) have shown that methods using simple shapes, like homogeneous spheres or spheroids, can be biased by orders of magnitude compared to DDA when the particle size is significantly larger than the wavelength.

The Rayleigh–Gans approximation (RGA; van de Hulst 1957) has been recently identified as a method that can be accurate enough for snowflake modelling (Tyynelä *et al.* 2013), yet simple enough to allow results to be derived from it in an analytic form, establishing a mathematical connection between the particle structure and the scattering properties. RGA is an approximation that ignores the interactions of the electromagnetic field between different parts of the scatterer, and is consequently usable when those interactions are negligible. The DDA–RGA intercomparison of Tyynelä *et al.* (2013) showed that, for unrimed snowflakes, the error of the RGA is small compared to T-Matrix or Mie scattering (van de Hulst 1957), which use homogeneous spheroidal and

spherical shapes, respectively. Leinonen *et al.* (2013) used the RGA theory to show that the statistical properties of the internal particle structure are responsible for the deficiencies of the spheroidal models which assume the particle volume to be filled with a homogeneous medium.

Unlike homogeneous medium approximations, the RGA theory is able to take the internal particle structure of arbitrary shaped particles into account. Hogan and Westbrook (2014) expanded the RGA for ensembles of snowflakes by assuming that snowflake structures are fractal by nature. The self-similarity assumption allowed them to derive an analytic expression for the ensemble averaged backscattering cross section; they called this method the "Self-Similar Rayleigh–Gans Approximation" (SSRGA). Very recently, Hogan *et al.* (2017) provided additional SSRGA expressions for the scattering phase function which makes the method also usable for simulations of passive microwave sensors.

If techniques such as SSRGA are to be used to analyze the scattering properties of snowflakes, it is crucial that the validity of RGA be examined. Triple-frequency radar signatures of snowfall have been found to be connected to particle size distribution and snowflake properties such as shape and bulk density (Leinonen *et al.* 2012; Kulie *et al.* 2014; Stein *et al.* 2015; Kneifel *et al.* 2015). They can be used as strong constraints for retrieval forward models, especially when the entire Doppler spectrum is analyzed (Kneifel *et al.* 2016). Comparisons made in the aforementioned studies for unrimed snowflakes clearly showed that the RGA and SSRGA are superior to spheroid-based methods that assume a homogeneous internal structure of the snowflake.

Riming (i.e. accretion and freezing of supercooled water droplets) of snowflakes is known to be an important microphysical process, which dramatically alters the properties of the snowflakes, and which is strongly correlated with the snow accumulation in mountainous terrain (e.g. Grazioli *et al.* 2015). It has not been previously investigated how riming of snowflakes, and the consequent change in morphology, affects the applicability of the Rayleigh–Gans theory. Stein *et al.* (2015) showed that the connection between RGA theory and the particle fractal dimension can explain the differences of the triple-frequency patterns of rimed and unrimed snowflakes. However, because the study of Tyynelä *et al.* (2013) only investigated unrimed snowflakes, it has not yet been established whether the RGA assumptions are valid for rimed snow. Riming greatly increases the density of snowflakes and makes their structure more homogeneous. These effects can be expected to increase the internal interactions of the electromagnetic field and hence potentially violate the key assumption of the RGA.

In this study, we use the RGA and SSRGA methods to analyze the rimed snowflake models created by Leinonen and Szyrmer (2015), who also computed the microwave scattering properties of those snowflakes using the DDA. We examine empirically the errors and biases that arise from using the RGA in place of the DDA method at frequencies of $13.6\ \mathrm{GHz}$ (Ku band), $35.6\ \mathrm{GHz}$ (Ka band) and $94.0\ \mathrm{GHz}$ (W band).

2. Data and methods

2.1. *Snowflake models*

In this study, we used the database of several thousand rimed aggregate snowflake models generated earlier by Leinonen and Szyrmer (2015); the details of the generation process can be found in that paper. The models were generated from volumetric, three-dimensional models of dendrite ice crystals using an algorithm that assembles these crystals into an aggregate. Each particle was held only at a single orientation, but their orientations were randomized.

Leinonen and Szyrmer (2015) simulated riming using three different scenarios. In model A, riming and aggregation occur simultaneously. In model B, all riming occurs after aggregation. Finally, in model C, there is only minimal aggregation and riming drives all snowflake growth. Models A and B were simulated at six different degrees of riming each, ranging from unrimed aggregates to heavily rimed particles that resemble graupel. For those models, the snowflakes maximum dimensions ranged up to $22\ \mathrm{mm}$, while for model C they reached $8\ \mathrm{mm}$. The degree of riming was quantified in that paper using the "effective liquid water path" (ELWP), which is the liquid water path that produces the simulated amount of riming, assuming a riming efficiency of 100%. Since we use the same dataset in this paper, we adopt this metric to distinguish between different amounts of riming.

While convenient for modeling purposes, ELWP is difficult to determine from measurements, and thus it may not be obvious which of our model datasets one should use. However, ELWP can be related empirically to the mass-dimensional relationship of the form $m = aD^b$: Leinonen and Szyrmer (2015) found similar exponents b for each ELWP with model A, and if we assume a constant value of b using the average of all model A datasets, we can relate the prefactor a to the ELWP as:

$$a = \begin{cases} 0.873 \times \mathrm{ELWP} + 0.0259, & 0 \le \mathrm{ELWP} < 0.1 \\ 0.355 \times \mathrm{ELWP} + 0.0777, & 0.1 \le \mathrm{ELWP} < 2.0, \end{cases} \quad (1)$$

$$b = 2.19 \quad (2)$$

where SI units are used for all quantities. Thus, the prefactor increases relatively quickly at the onset of riming and then grows almost linearly as a function of ELWP.

The riming models appear to provide a good approximation of the conditions found in nature. Model C produced mass–dimensional (m–D) relationships comparable to that found for graupel by Heymsfield and Wright (2014). For the low end of the snowflake density range, Leinonen and Moisseev (2015) showed that the unrimed model aggregates have m–D relationships close to those of Mitchell *et al.* (1990). Examples of the particles can be found in Fig. S18 of the supporting information accompanying this article, as well as Fig. 1 of Leinonen and Szyrmer (2015). The m-D relations derived for each model and ELWP separately were given in Fig. 2 of Leinonen and Szyrmer (2015), and therefore will not be reproduced here.

Models A and B produced very similar scattering results in Leinonen and Szyrmer (2015), and the RGA also behaved similarly for those models. Hence, in the interest of brevity, we only show the results for models A and C. The results for model B can be found in the supporting information accompanying this article.

2.2. *Scattering properties*

The complete description of the scattered wave in the far field is given by the complex amplitude scattering matrix $\mathbf{S}$. Using the notation of Bohren and Huffman (1983), at scattering zenith angle θ and azimuth angle ϕ, $\mathbf{S}$ is

$$\mathbf{S}(\theta, \phi) = \begin{bmatrix} S_2 & S_3 \\ S_4 & S_1 \end{bmatrix}. \quad (3)$$

The scattering properties compared in this article are the backscattering cross section C_{bsc}, the scattering cross section C_{sca}, the absorption cross section C_{abs} and the asymmetry parameter g. These are derived from the amplitude scattering

matrix as

$$C_{\rm bsc} = \frac{2\pi}{k^2}\left(|S_1(\pi,0)|^2+|S_2(\pi,0)|^2\right) \quad (4)$$

$$C_{\rm sca} = \frac{1}{2k^2}\int_0^{2\pi}\int_0^{\pi}\left(|S_1(\theta,\phi)|^2+|S_2(\theta,\phi)|^2\right)\sin\theta\,{\rm d}\theta{\rm d}\phi \quad (5)$$

$$C_{\rm abs} = \frac{2\pi}{k^2}\left({\rm Re}[S_1(0,0)+S_2(0,0)]\right) \quad (6)$$

$$g = \frac{1}{2k^2C_{\rm sca}}\int_0^{2\pi}\int_0^{\pi}\left(|S_1(\theta,\phi)|^2+|S_2(\theta,\phi)|^2\right)\sin\theta\,\cos\theta\,{\rm d}\theta{\rm d}\phi. \quad (7)$$

where the wavenumber $k=2\pi\lambda^{-1}$ and λ is the wavelength. The backscattering cross section of snowflakes is the most important property for radar retrievals. The attenuation of the radar signal is also dependent on the extinction cross section $C_{\rm ext}=C_{\rm sca}+C_{\rm abs}$. Furthermore, the extinction and scattering cross sections as well as the asymmetry parameter are needed in radiative transfer calculations used to model multiple scattering in radar systems, and the brightness temperatures observed by passive microwave radiometers.

2.3. *Rayleigh–Gans Approximation (RGA)*

The Rayleigh–Gans Approximation (RGA) is a theory based on the assumption that the electromagnetic interactions between parts of the scatterer are negligible. The scattered wave is hence modelled relatively simply as a superposition of waves scattered from different parts of the scattering particle. Here, we give an overview of the theory; more details can be found in Bohren and Huffman (1983), whose notation we use throughout this paper.

The RGA theory modifies the Rayleigh scattering law (van de Hulst 1957) to incorporate the interference of out-of-phase scattered waves originating from various parts of the scatterer. The amplitude scattering matrix given by RGA is

$$\mathbf{S}(\theta,\phi) = \begin{bmatrix} S_2 & 0 \\ 0 & S_2\cos\theta \end{bmatrix} \quad (8)$$

$$S_2 = \frac{3i}{4\pi}K_{\rm NS}k^3Vf \quad (9)$$

where i is the imaginary unit, V is the total volume of the material in the scattering particle, f is the Rayleigh–Gans form factor and $K_{\rm NS}$ is the modified Clausius–Mossotti factor that is discussed in Sect. 2.4.

The form factor f describes the degree of coherence of the scattered waves. It is a dimensionless number

$$f = \frac{1}{V}\int_V \exp(i\delta(\mathbf{R}))\,{\rm d}\mathbf{R} \quad (10)$$

$$\delta(\mathbf{R}) = \mathbf{R}\cdot(\mathbf{k}_{\rm inc}-\mathbf{k}_{\rm sca}) \quad (11)$$

where $\mathbf{R}$ is the position within the particle and δ depends on the phase difference between the incident wave vector $\mathbf{k}_{\rm inc}$ and scattered wave vector $\mathbf{k}_{\rm sca}$. Note that the integration domain in Eq. (10) only includes the ice in the snowflake; the air parts are not considered and thus no effective medium approximation is necessary. The RGA reduces to the Rayleigh scattering theory when the dimensions of the scatterer are small compared to the wavelength, and all scattered waves are in phase. In that case, $\delta\to 0$ and consequently $f\to 1$. In this study, we used snowflake models made of small volume elements, and thus adopted the following discretization for the numerical computation of Eq. (10)

$$f = \left(\sum_{k=1}^{N_{\rm elem}}V_k\right)^{-1}\sum_{k=1}^{N_{\rm elem}}V_k\exp(i\delta(\mathbf{R}_k)) \quad (12)$$

where $N_{\rm elem}$ is the number of volume elements and V_k is the volume of each element. Besides being simple and efficient to compute, this discretization is the same as that performed in DDA (see Sect. 2.6) for the solution of the volume integral equation. Thus, the RGA and DDA were computed in equivalent ways and the only difference is that the internal interactions are considered in DDA, while they are neglected in RGA.

The applicability of the RGA is typically considered to require that

$$|m_{\rm eff}-1| \ll 1 \quad (13)$$

$$2kD|m_{\rm eff}-1| \ll 1 \quad (14)$$

where D is the maximum diameter of the particle. These requirements mean that the particles are assumed to be optically soft and not too large, and that each volume element is only excited by the incident field. For ice at microwave frequencies, the real part of $m_{\rm eff}-1$ is much larger than the imaginary part, and thus dominates the absolute value in Eqs. (13) and (14). Berry and Percival (1986) predicted, and Tyynelä *et al.* (2013) showed in the case of unrimed snowflakes, that these requirements can be greatly relaxed for sparse aggregates. This is because the effective refractive index of the ice–air mixture, rather than that of pure ice, can be used for $m_{\rm eff}$ for the purpose of determining the validity of RGA. As aggregate snowflakes become denser with riming, the validity can be expected to weaken. The focus of the present work is to investigate the errors thus introduced.

2.4. *Adjustment of RGA for nonspherical monomers*

The Clausius–Mossotti factor K, which appears in Eq. (9), is classically defined as

$$K = \frac{m^2-1}{m^2+2}. \quad (15)$$

The complex refractive index m depends on the material (e.g. ice or liquid water) and is also a function of temperature and frequency; we use the values published by Warren and Brandt (2008). However, it has long been known (e.g. van de Hulst 1957) that non-spherical scatterers require adjustments to Rayleigh scattering theory because their polarizability differs from that of spheres, and may in fact be anisotropic. Such modifications have been adopted in various geophysical applications by, for example, Seliga and Bringi (1976) for radar measurements of raindrops, Westbrook (2014) for ice clouds, and by Battaglia *et al.* (1999) for Gaussian particles.

When an ensemble of nonspherical scatterers is randomly oriented, their total polarizability is isotropic. Importantly, this is the case for aggregate snowflakes composed of many nonspherical, randomly oriented ice monomers. As discussed by Hogan *et al.* (2017), in such circumstances it is convenient to account for the nonspherical monomers by adopting a modified K factor that has been adjusted for the nonsphericity. The modified K, denoted as $K_{\rm NS}$ by Hogan *et al.* (2017), is defined as the polarizability of the monomer divided by its volume. For spherical monomers, this definition is equivalent to the K of Eq. (15). On the other hand, for strongly nonspherical ice monomers like plates or columns, $K_{\rm NS}$ can be significantly different from K. Westbrook (2014) used DDA simulations to derive approximations of $K_{\rm NS}$ for hexagonal plates, columns, and dendrites as a function of their aspect ratio and volume fraction of ice.

Hogan *et al.* (2017) showed that if an aggregate snowflake is composed of ice monomers with a specific size and aspect ratio, using $K_{\rm NS}$ leads to much better agreement with DDA than using the classical K. In this study, the aggregates were somewhat more

complex because they had been built from a size distribution of dendrites with size-dependent aspect ratios. In addition, the rimed ice added to the particles further changes the monomer properties depending on the degree of riming. Hence, an exact theoretical correction was difficult to derive. We instead estimated K_{NS} by comparing the volume-normalized absorption cross section C_{abs}/V derived from RGA and DDA for unrimed snowflakes at Ku, Ka, and W-bands. As shown in Hogan *et al.* (2017), C_{abs}/V for RGA is only a function of the imaginary part of K_{NS} and independent of the form factor.

We obtained the best agreement of C_{abs}/V with DDA assuming hexagonal plates with an aspect ratio of 0.3. This value is larger than the average aspect ratio of the ice crystals used, 0.12, but the riming and the complex dendrite shapes of our ice crystals can be expected to affect the effective aspect ratio. Furthermore, we shall show in Sect. 3.1 that with a K_{NS} derived using this adjustment, the backscattering and scattering cross sections also agreed well between RGA and DDA at the Ku band (Rayleigh scattering regime). This indicates that the real part of K_{NS} is also approximated well using this adjustment. The resulting value for $|K_{\mathrm{NS}}|^2$ — a value which is linearly related to the RGA scattering and backscattering cross sections — is 0.21 (almost independent of frequency) compared to a value of 0.18 obtained when using Eq. (15) with the m for pure ice. A similar value of 0.22 was obtained for columns with aspect ratio of 4 used by Hogan *et al.* (2017).

2.5. *Self-Similar Rayleigh–Gans Approximation (SSRGA)*

The Self-Similar Rayleigh–Gans Approximation is based on the RGA and was developed by Hogan and Westbrook (2014). They provided an analytic expression for the average backscattering cross section of an ensemble of unrimed snow aggregates for microwave frequencies. The method has been recently refined and extended by Hogan *et al.* (2017), who also provide expressions for the full scattering phase function, absorption and scattering cross sections, as well as the asymmetry parameter.

The SSRGA requires five parameters that describe the decomposition of the mean structure and the fluctuations of mass distributed along a certain direction. In this study, these parameters have been derived following the method described in Hogan *et al.* (2017) for unrimed and rimed snow aggregates (riming model A and C, as well as model B shown in the supporting information); the derived SSRGA parameters are discussed in Sec. 3.2.

2.6. *Discrete Dipole Approximation*

The reference method used in this paper is the Discrete Dipole Approximation (DDA Flatau and Draine 1994), which models the complete interactions between various parts of the scatterer by dividing it into small homogeneous volume elements (which behave as dipoles), and solving the resulting linear system of equations. With the combination of fast Fourier transforms for computing convolutions and iterative methods for solving linear systems of equations, very large systems (up to $N \approx 10^9$) can be solved (Goodman *et al.* 1991).

The accuracy of DDA is generally limited only by the size of the dipoles. Generally, the individual dipoles must be much smaller than the wavelength inside the scattering particle. Various heuristic criteria have been published to establish the maximum permissible dipole size that still yields acceptable results. According to Zubko *et al.* (2010), $|m|kd < 0.5$ is a sufficient criterion; for us, this relative size was largest at W band with $|m|kd = 0.14$, well below the limit.

The DDA implementation we used in this work was ADDA (Yurkin and Hoekstra 2011). The ADDA output includes the amplitude matrix $\mathbf{S}$ for every scattering angle, and from that information, the scattering properties used here can be computed. The details of the DDA setup were described by Leinonen and Szyrmer (2015).

3. Results and discussion

3.1. *Rayleigh–Gans Approximation*

We show the RGA biases of the scattering properties in Fig. 1 (C_{bsc}), Fig. 2 (C_{sca}), Fig. 3 (C_{abs}) and Fig. 4 (g). In these figures, the size-dependent bias of RGA (shown as continuous lines) has been estimated with a running mean using a Gaussian weighting function. Since this article is focused on radar applications, we report the biases for C_{bsc}, C_{sca} and C_{abs} in decibels, which are commonly used in the radar context. In order to make it easier to compare between the magnitudes of the biases of different variables, decibels are also used for the biases of C_{sca} and C_{abs}, even though these variables are not typically given in logarithmic units. The reported bias in dB is thus

$$10 \log_{10} \left(\frac{C_{\mathrm{RGA}}}{C_{\mathrm{DDA}}} \right), \tag{16}$$

where C_{RGA} and C_{DDA} can be any of C_{bsc}, C_{sca} or C_{abs}. For example, 1 dB corresponds to approximately 26% relative difference, while 3 dB is roughly a factor of 2. For g, linear units are used instead and the bias is given as $g_{\mathrm{RGA}} - g_{\mathrm{DDA}}$. The absolute changes in the parameters can be seen in Figs. 6–9.

Inspection of Fig. 1 reveals that the RGA bias of the backscattering cross section for individual particles at single orientations increases with the degree of riming when the particles are sufficiently large compared to the wavelength. This is clearest at the W band (Fig. 1c), where the unrimed and lightly rimed snowflakes are concentrated relatively close to zero bias, while the most heavily rimed snowflakes (brown diamonds) are spread throughout the shown range of -25 to $+15$ dB. The dramatic increase in the spread with riming is in contrast to the variability of single-orientation backscattering cross sections at the W band between snowflakes of similar size and mass: this variability is nearly independent of riming at roughly ± 10 dB (Fig. 4 of Leinonen and Szyrmer 2015). Interestingly, then, for lightly rimed snowflakes the variability of the RGA bias is much smaller than the natural variability of the backscattering cross section, while for heavily rimed particles it is actually much larger.

The spread in the bias for individual particles widens rapidly at snowflake sizes larger than the wavelength, and at somewhat smaller sizes for the graupel-like particles produced by riming model C. The model C particles also exhibit a significant spread at somewhat smaller sizes than those from model A. Without the adjustment that results in the K_{NS} factor, a small bias of approximately -0.4 dB, or 10%, would persist even at small snowflake sizes, but this is largely fixed by the adjustment we have made, as explained in Sect. 2.4. Such a bias was previously noted by Tyynelä *et al.* (2013), who attributed it to the inaccuracy of the Rayleigh scattering theory for elongated shapes; the success of our adjustment in removing this bias suggests that their explanation was, in fact, correct, and that the K factor adjustment can be used to eliminate the residual bias arising from this.

The mean RGA bias of C_{bsc} also becomes more negative with increased riming at small size–wavelength ratios, but this effect is modest compared to the increase in the spread. Only for the most heavily rimed particles (model A at $2.0\ \mathrm{kg\,m^{-2}}$ and model C) at the W band does the mean negative bias significantly exceed 1 dB. The model A bias exhibits no significant pattern besides becoming somewhat more negative with increasing size. Model C, on the other hand, appears to oscillate at diameters larger than

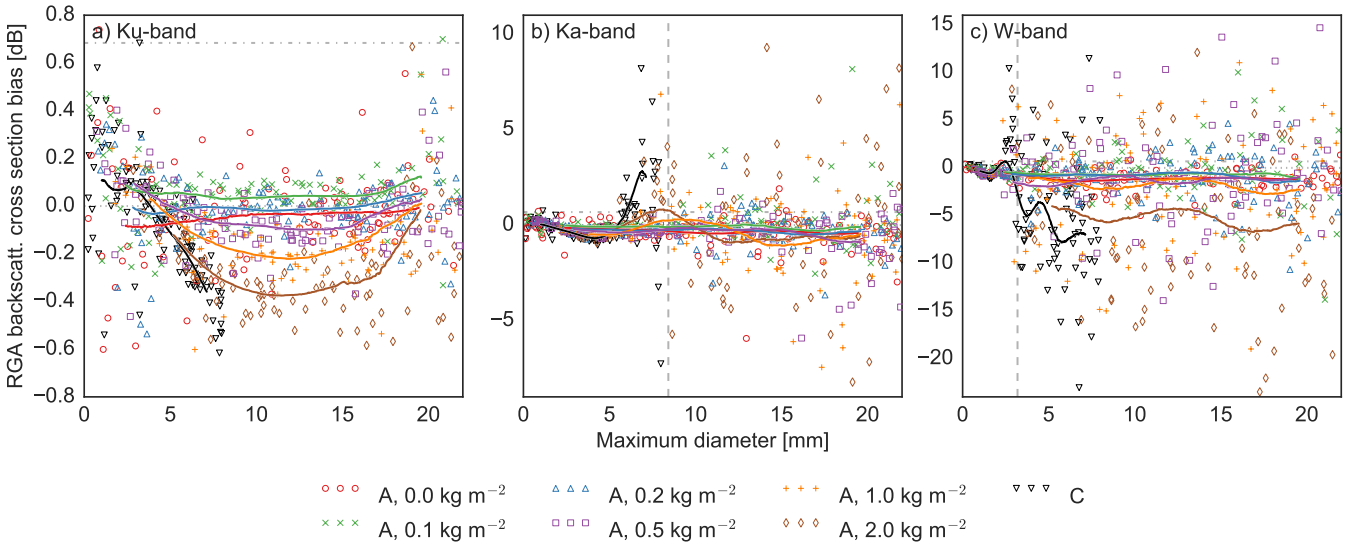

Figure 1. The RGA backscattering cross section (C_{bsc}) bias (RGA minus DDA) vs. the maximum diameter of the snowflakes. Note the different bias scales in the plots. The markers indicate the bias for individual particles at a single orientation; for clarity, only one out of every five particles is shown. The colour and shape of the markers indicate the riming amount (expressed in terms of the effective liquid water path, in $\mathrm{kg\,m^{-2}}$) and model (as per Leinonen and Szyrmer 2015). The coloured curves show the running mean biases for the corresponding dataset, the vertical line indicates the wavelength, and the horizontal grey line indicates where the zero point would be if the unadjusted K factor was used. (a) For the Ku band. (b) For the Ka band. (c) For the W band.

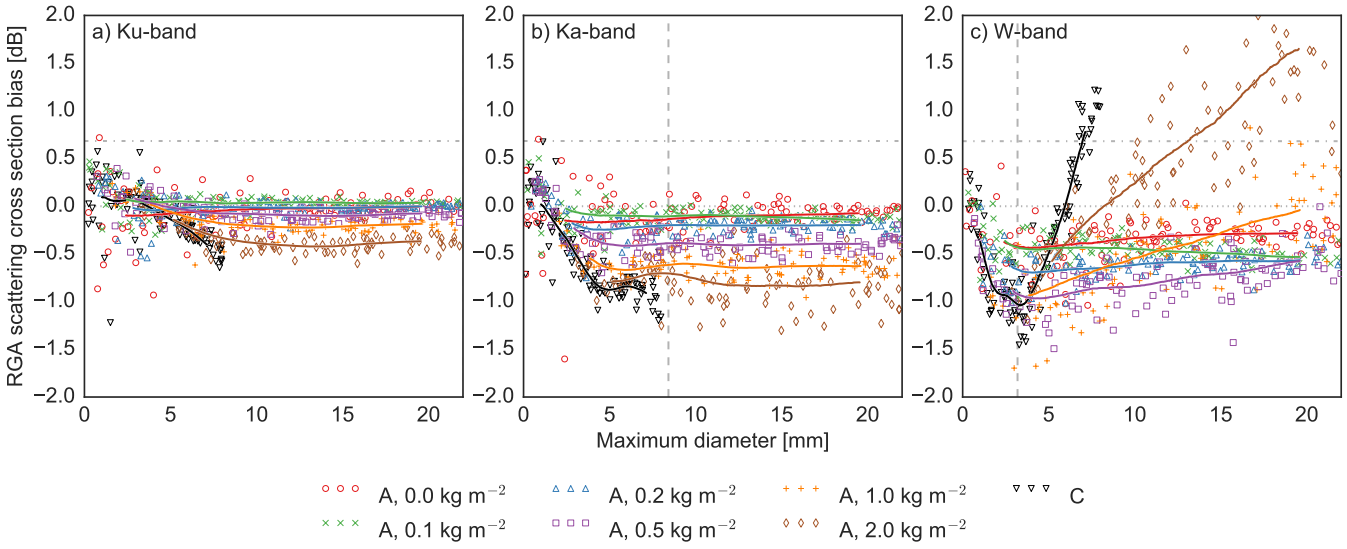

Figure 2. As Fig. 1, but for the scattering cross section C_{sca}.

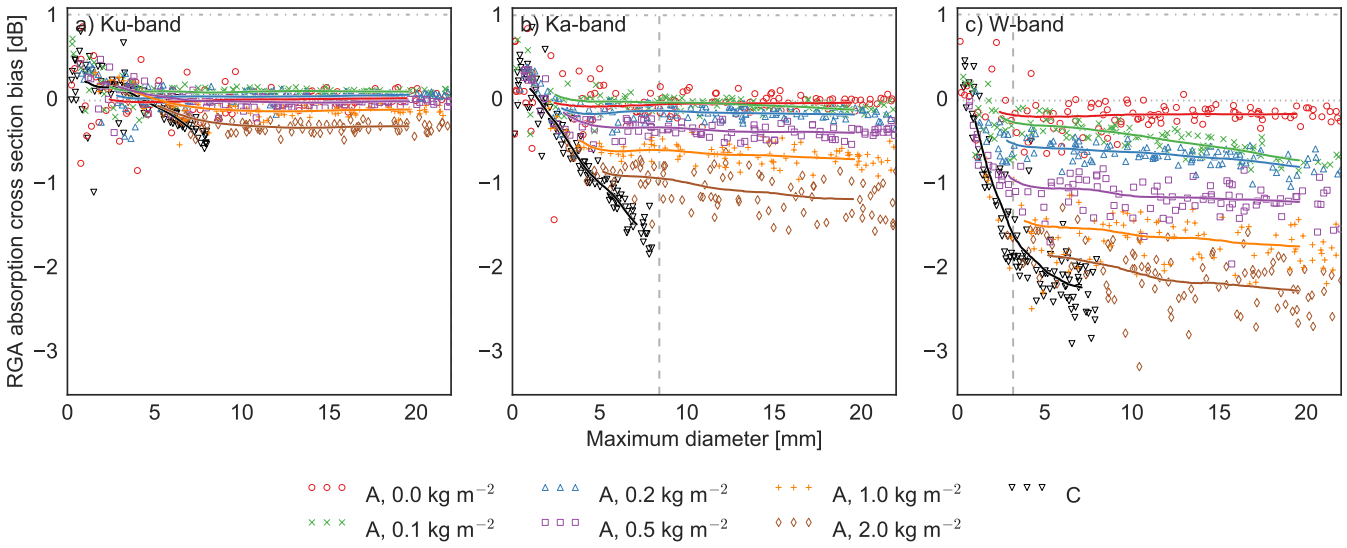

Figure 3. As Fig. 1, but for the absorption cross section C_{abs}.

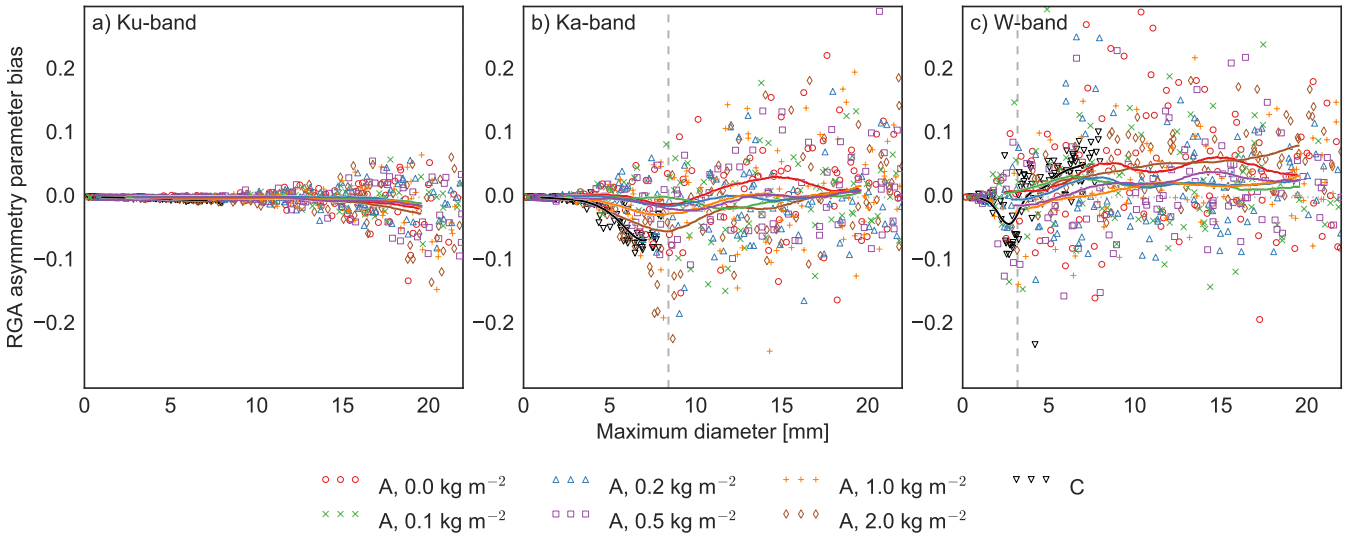

Figure 4. As Fig. 1, but for the asymmetry parameter g, and the bias is given in linear units rather than decibels.

$\lambda/2$ for both the Ka and W bands. This hints at a resonance effect that causes the particle internal interactions to change. Because the average bias is small for all but the most heavily rimed snowflakes, the applicability of the RGA can be greatly extended in practice. Remote sensing devices measure the sum of signals from a large number of hydrometeors, and thus errors with individual particles are effectively averaged out.

The single-snowflake biases for C_{sca} (Fig. 2) are less scattered than those for C_{bsc}. The absolute values of the bias are also smaller, especially for the W band. Figs. 2a–b reveal a consistently more negative bias with increased riming; this effect is most pronounced at the Ka band. Above a snowflake diameter of approximately $5\ \mathrm{mm}$, the mean bias hardly varies with size, which is consistent with the findings of Tyynelä *et al.* (2013). However, for the W band, Fig. 2c shows an interesting pattern for the most heavily rimed particles: their bias shifts rapidly to more positive values once the particle size becomes large enough. This feature is clearest for the model C snow particles, for which the bias is remarkably consistent as a function of size.

The behavior of the bias of C_{abs} (Fig. 3) is more consistent than that of C_{bsc} or C_{sca}. At all wavelengths, there is a steady, gradual increase in the negative bias of RGA with increasing riming. The magnitude of the bias effect is similar to that of C_{sca}, but it becomes quite steadily larger with increased riming. The rapid size-dependent increase in the bias for heavily rimed snowflakes at the W band in C_{sca} is absent from the behavior of the C_{abs} bias, which is relatively constant even at the W band.

In contrast to the cross sections, the bias in g (Fig. 4) does not appear to be significantly dependent on the amount of riming. The bias is near zero for small particle sizes, and begins to exhibit spread at snowflake diameters larger than $\lambda/2$. There is no discernible pattern to the spread for model A, but model C appears to have an increasingly negative bias between $\lambda/2$ and λ at the Ka and W bands, quickly shifting to a slightly positive bias at sizes larger than λ (W band only). This is likely caused by the same resonance effect that is responsible for the patterns in C_{bsc} and C_{sca}.

3.2. *Self-Similar Rayleigh–Gans Approximation*

The SSRGA is formulated using five parameters, as defined by Hogan *et al.* (2017): α_{eff}, κ, β, γ and ζ_1. Their roles are described in more detail below. Each parameter has been derived for all particle types with different ELWP and within $1.5\ \mathrm{mm}$ wide size bins. The derived parameters are shown as a function of size in Fig. 5.

The effective aspect ratio $\alpha_{\mathrm{eff}} = d/D$ is the ratio between the particle extent d in the direction of the propagating wave (in this study, always assumed to be along the vertical axis), and the maximum particle extent D. The aspect ratios are mostly between 0.6 and 0.7, which is a typical range also found in in-situ observations and snowflake growth models (Korolev and Isaac 2003; Westbrook *et al.* 2004a; Hogan *et al.* 2012).

As expected, the aspect ratio increases with riming. This effect is largest for the smaller size range because even a small number of droplets freezing onto the small aggregate cause the shape to become more round, and aspect ratios can be up to 0.9. In contrast, for the largest aggregates of model A, even the strongest riming does not significantly change the overall aggregate structure, and the aspect ratios remain between 0.65 and 0.7. Riming model C produces the aspect ratios closest to 1 (around 0.85–0.9), even at small sizes. This can be explained by the generation process, in which only a small number of single crystals grows only due to continuous riming.

The kurtosis parameter κ describes the shape of the average mass distribution along the direction of propagation. A Gaussian distribution would yield $\kappa = 0$; a positive value indicates that the mass distribution has a sharp peak in the centre along with significant tails, and a negative κ denotes a more "flat-topped" distribution. Our κ values found for the rimed aggregates with different ELWPs range between 0.1 and 0.25. This range, and also the near independence of size, is very similar to the results found for the two aggregate models analyzed in Hogan *et al.* (2017).

The fluctuations of mass around the average structure are described by the remaining three parameters β, γ, and ζ_1. After subtracting the average mass structure, a Fourier-like decomposition is applied to the fluctuations. At wavenumbers that correspond to the size range where the particle structure is self-similar, the spectrum of the mass fluctuations closely follows a power law (Sorensen 2001; Hogan and Westbrook 2014). We were able to fit such a power law even at the highest ELWP values. The self-similarity assumption thus appears sufficiently valid (or at least phenomenologically correct) also for our largest degrees of riming; an exception is the size range below $3\ \mathrm{mm}$, which we excluded from the analysis.

The prefactor of the power law is β, which describes the amplitude of the fluctuations, while γ is the exponent of the fit indicating how fast the amplitude of mass fluctuations decreases

with larger wavenumbers (smaller sizes). For fractal particles, the slope parameter γ is closely related to the fractal dimension (Sorensen 2001). Our results seem to confirm this interpretation since we found a gradual increase of γ with riming from a value close to 2 to values between 2.5 and 3.7. A fractal dimension of 2 is typical for unrimed aggregates both simulated and observed (e.g. Westbrook *et al.* 2004a,b; Schmitt and Heymsfield 2010). Values closer to 3 are expected from a more homogeneously filled structure similar to our most heavily rimed aggregates. It is also interesting to see in Fig. 5b that for moderate ELWP (e.g. $0.5\ \mathrm{kg\,m^{-2}}$), γ is very size dependent, while the values become nearly constant with size for non-riming and maximum riming conditions.

The β parameter shows a significant variability as soon as the aggregates become rimed. At medium ELWPs we found β to peak at around 10 times higher values compared to the remaining size range and to unrimed aggregates. It seems likely that this behavior is related to the change of internal mass fluctuations, but currently we are unable to provide a thorough explanation.

The third parameter ζ_1 only affects the first wavenumber of the spectrum and shows only a slight increase with size and a decrease with ELWP. Overall, the range of values found for all SSRGA parameters derived for the unrimed aggregates is within the range found by Hogan *et al.* (2017).

The ensemble scattering properties derived with the SSRGA are compared in Figs. 6–9 with the RGA computations for the individual particles. Although individual particles calculated with RGA show occasional large deviations from the ensemble SSRGA scattering properties — especially for backscattering (Fig. 6) — the SSRGA fits the RGA scattering properties very well. This result is in general agreement with the comparisons of SSRGA and RGA for unrimed aggregates presented in Hogan *et al.* (2017). It is an interesting finding of this study that the SSRGA approximates all scattering parameters of the RGA very well even for the highest degrees of riming, where the assumption of self-similarity might become less valid due to the mixing of different growth processes (aggregation and riming).

4. Conclusions

In this paper, we examined the applicability of the Rayleigh–Gans Approximation (RGA) and the Self-Similar Rayleigh–Gans Approximation (SSRGA) for the calculation of microwave scattering properties of snowflakes. As reference method, we used the discrete dipole approximation (DDA). The focus of this work was to determine whether the RGA remains useful with the introduction of riming, and whether SSRGA is able to capture the properties of RGA for rimed snowflakes.

We found that the RGA is subject to increasing errors with larger particle sizes, shorter wavelengths and higher degrees of riming. For individual particles, especially at the W-band, there are rather large differences between the RGA and DDA methods already for moderate riming. The errors of the backscattering cross section are particularly large compared to the more modest biases of the scattering and absorption cross sections. On the other hand, the systematic errors are small for all but the most heavily rimed snowflakes: the average bias is at most $1\ \mathrm{dB}$ except for model A at $\mathrm{ELWP} = 2.0\ \mathrm{kg\,m^{-2}}$ (the largest amount of riming used in the dataset), and for the graupel-like model C. Thus, for realistic scenarious where a large number of snowflakes is observed simultaneously, the errors attributed to the use of RGA are typically smaller than those resulting from uncertainties in the snowflake shape and density (for an evaluation of the latter, see e.g. Mace and Benson 2017; Xu and Mace 2017).

We were able to reduce the small, constant biases found in RGA by estimating a constant adjustment to the Clausius–Mossotti factor K. The adjustment is based on matching the absorption cross sections given by DDA and RGA, but it was also able to nearly eliminate biases in the backscattering and scattering cross sections. This suggests that the non-sphericity of the ice crystals was responsible for the small constant biases reported by Tyynelä *et al.* (2013), and this type of adjustment can be used to correct for them. Unfortunately, this adjustment required analysis of the already-known DDA scattering properties, and it is not obvious how the adjustment factor should be estimated by those researchers who wish to use RGA or SSRGA without resorting to DDA calculations. As a first approximation, we suggest that they use our adjusted value of $|K_{\mathrm{NS}}|^2 = 0.21$, although the exact value depends on the ice crystal type. This value is almost constant over the microwave wavelength range. On the other hand, $\mathrm{Im}[K_{\mathrm{NS}}]$, which determines the absorption, is wavelength-dependent, but can be calculated for a given wavelength using the method of Westbrook (2014) for hexagonal plates with an aspect ratio of 0.3.

Based on our results, we recommend that DDA be used as the reference method of choice for snowflake scattering calculations when the available computational resources permit it. The RGA and SSRGA are viable alternatives for unrimed as well as lightly or moderately rimed snowflakes, especially in the usual case where many snowflakes are observed simultaneously, and the individual scatterers are averaged out. Only with the most heavily rimed snowflakes do the RGA and SSRGA display significant systematic biases. For the graupel-like particles of model C, Leinonen and Szyrmer (2015) showed that the T-matrix calculations for spheroidal particles can estimate the backscattering properties quite accurately, even though for unrimed snow the spheroid model was very inaccurate. This considered, given a choice between RGA or the T-matrix method, RGA is probably more appropriate for the majority of icy hydrometeors, but for backscattering from graupel particles it may, in fact, be preferable to use the spheroid model and the T-matrix method.

The SSRGA approximates the RGA results very well for all scattering parameters and degrees of riming. Considering that most remote sensors measure the average scattering properties of a certain particle ensemble within their measuring volume, the SSRGA seems to be a valuable method for calculating these ensemble scattering properties. The most appealing aspect of the RGA and SSRGA, besides their fast computation, is that they directly relate the structural properties of the particles to their scattering properties.

A better understanding of the limitations of the RGA and SSRGA, which are mainly a result of the scattering interactions of the internal particle elements, will help exploit their potential as a fast scattering approximation for radiative transfer calculations of active and passive microwave sensors. It also seems to be possible to find a sufficient correction for at least some of the biases found for RGA and SSRGA in previous studies, but this will require a more in-depth study including different aggregate monomers.

Modern in-situ instrumentation that allows one to investigate snowflake structure, as well as aggregation and riming models, are vital for better constraining the possible range of variability of snow structure parameters. These constraints can then be directly linked to the scattering properties with methods like the RGA or SSRGA.

Acknowledgements

We thank three anonymous reviewers for their constructive comments. The research of JL was carried out at the Jet Propulsion Laboratory, California Institute of Technology, under contract with NASA. His work was supported by the NASA Aerosol Cloud Ecosystem mission under RTOP WBS 103930/6.1. JL

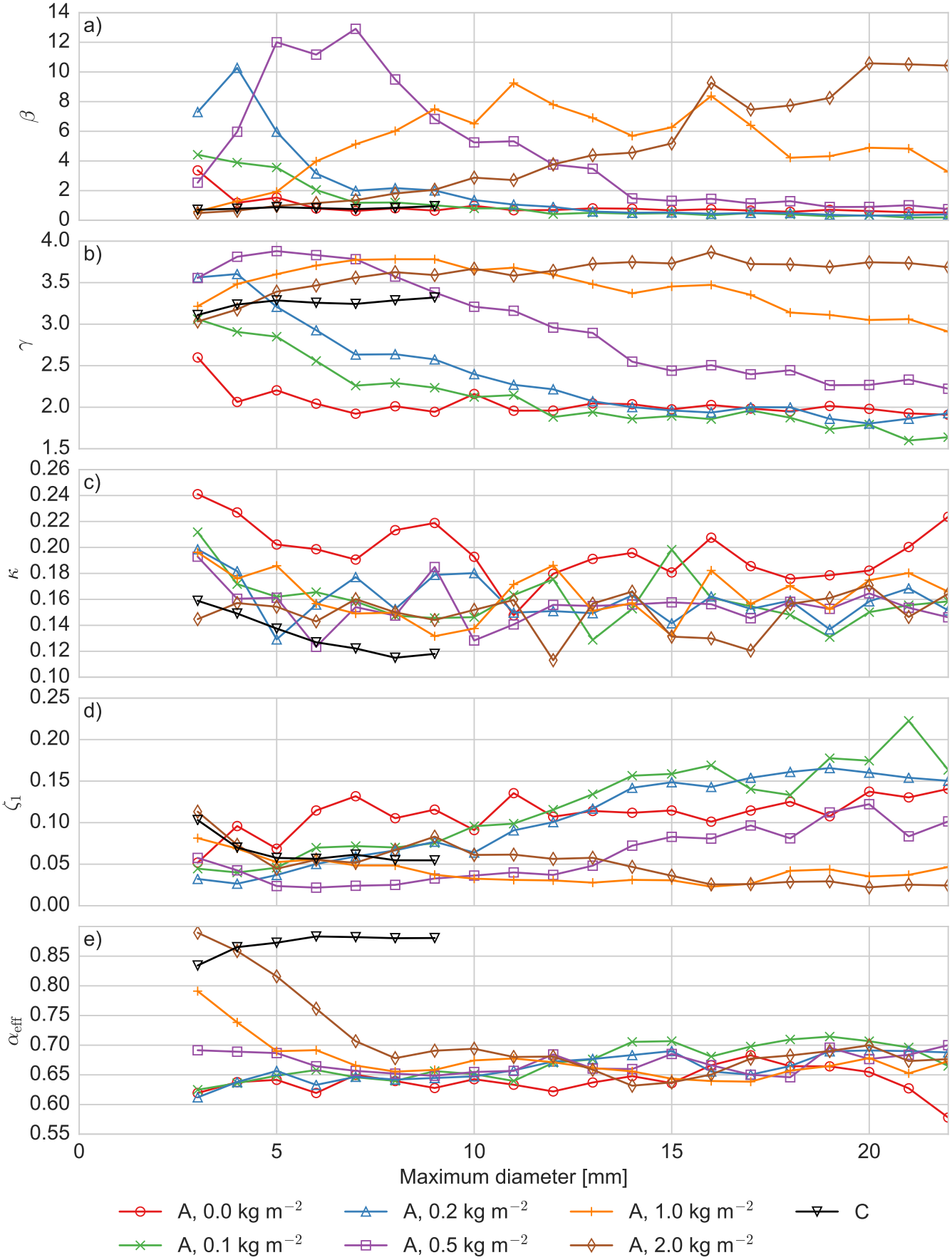

Figure 5. Coefficients of the SSRGA derived for rimed dendrite aggregates (Leinonen and Szyrmer 2015) with different ELWP and for 1.5 mm wide particle size bins (with approximately 60 particles per bin), following the method described by Hogan *et al.* (2017). The meaning of the different coefficients is described in the text.

was funded under subcontract #1559252 from the Jet Propulsion Laboratory to UCLA. Contributions from SK were carried out within the Emmy-Noether Group OPTIMIce funded by the German Research Foundation (DFG) under grant KN 1112/2-1. JJL and SK also acknowledge travel support from the Transregional Collaborative Research Centre SFB/TR172 "ArctiC

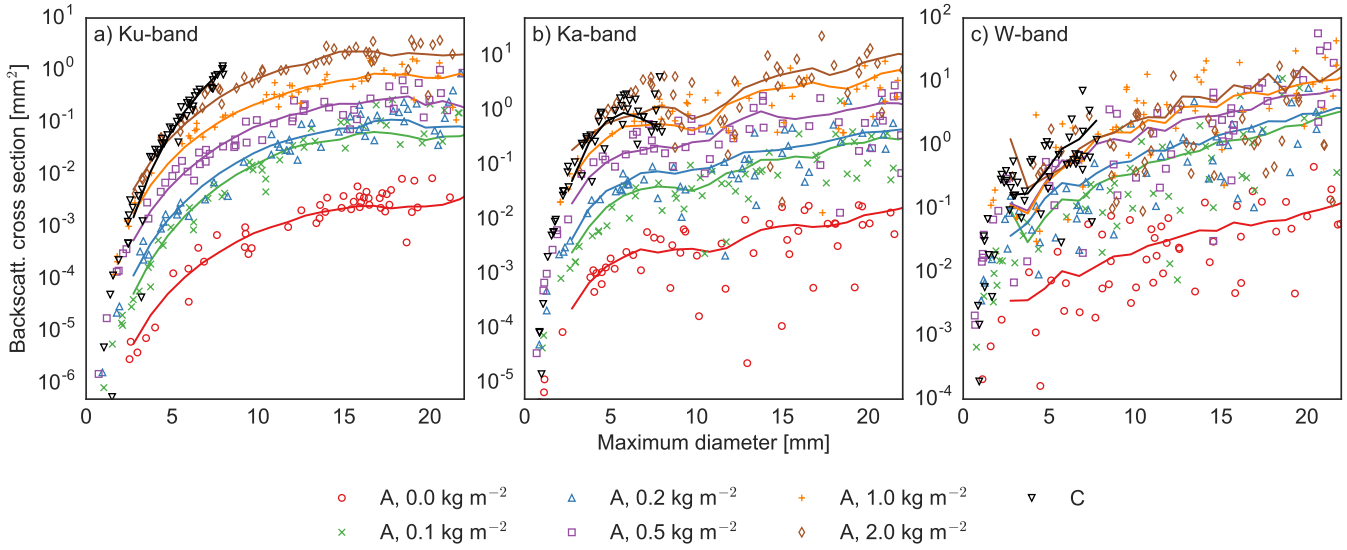

Figure 6. The backscattering cross section (C_{bsc}) for the Rayleigh–Gans and Self-Similar Rayleigh–Gans approximations. The individual markers correspond to the cross-sections calculated directly using RGA, while the lines are given by SSRGA. The colour and shape of the lines and markers are the same as with Fig. 1. (a) For the Ku band. (b) For the Ka band. (c) For the W band.

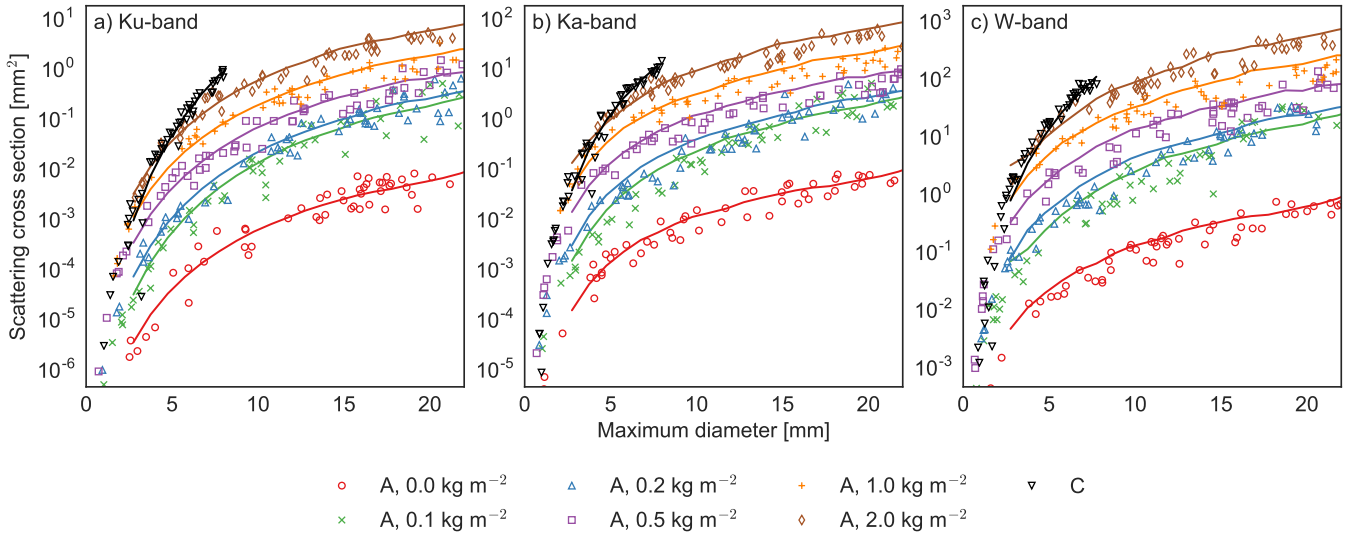

Figure 7. As Fig. 6, but for the scattering cross section C_{sca}.

Amplification: Climate Relevant Atmospheric and SurfaCe Processes, and Feedback Mechanisms (AC)^3".

Supporting Information

The supporting information file accompanying this article presents Figs. S1–S18. Figs. S1–S9, are equivalent to Figs. 1–9 in this article, but instead show data generated using the riming model B of Leinonen and Szyrmer (2015). Figs. S10–S13 show alternative versions of Figs. 1–4 using the mass-equivalent diameter on the horizontal axis instead of the maximum diameter. Figs. S14–S17 contain versions of the same plots using the size parameter on the vertical axis instead. Fig. S18 shows examples of the various snowflakes generated using our model.

References

Battaglia A, Muinonen K, Nousiainen T, Peltoniemi J. 1999. Light scattering by Gaussian particles: Rayleigh-ellipsoid approximation. *J. Quant. Spectrosc. Radiat. Transfer* **63**(2–6): 277–303, doi:10.1016/S0022-4073(99)00020-5.

Berry M, Percival I. 1986. Optics of fractal clusters such as smoke. *Opt. Acta* **53**: 577–591, doi:10.1080/713821987.

Bohren CF, Huffman DR. 1983. *Absorption and scattering of light by small particles*. John Wiley & Sons, Inc.: New York, USA.

Field PR, Heymsfield AJ. 2015. Importance of snow to global precipitation. *Geophys. Res. Lett.* **42**(21): 9512–9520, doi:10.1002/2015GL065497.

Flatau PJ, Draine BT. 1994. Discrete-dipole approximation for scattering calculations. *J. Opt. Soc. Am. A* **11**: 1491–1499, doi:10.1364/JOSAA.11.001491.

Goodman JJ, Draine BT, Flatau PJ, *et al.* 1991. Application of fast-Fourier-transform techniques to the discrete-dipole approximation. *Opt. Lett.* **16**(15): 1198–1200, doi:10.1364/OL.16.001198.

Grazioli J, Lloyd G, Panziera L, Hoyle CR, Connolly PJ, Henneberger J, Berne A. 2015. Polarimetric radar and in situ observations of riming and snowfall microphysics during CLACE 2014. *Atmos. Chem. Phys.* **15**(23): 13 787–13 802, doi:10.5194/acp-15-13787-2015.

Heymsfield A, Wright R. 2014. Graupel and hail terminal velocities: Does a "supercritical" Reynolds number apply? *J. Atmos. Sci.* **71**: 3392–3403, doi:10.1175/JAS-D-14-0034.1.

Hogan RJ, Honeyager R, Tyynelä J, Kneifel S. 2017. Calculating the millimetre-wave scattering phase function of snowflakes using the Self-Similar Rayleigh-Gans Approximation. *Quart. J. Roy. Meteor. Soc.* **143**, doi:10.1002/qj.2968.

Hogan RJ, Tian L, Brown PRA, Westbrook CD, Heymsfield AJ, Eastment JD. 2012. Radar scattering from ice aggregates using the horizontally aligned oblate spheroid approximation. *J. Appl. Meteor. Climatol.* **51**: 655–671, doi:10.1175/JAMC-D-11-074.1.

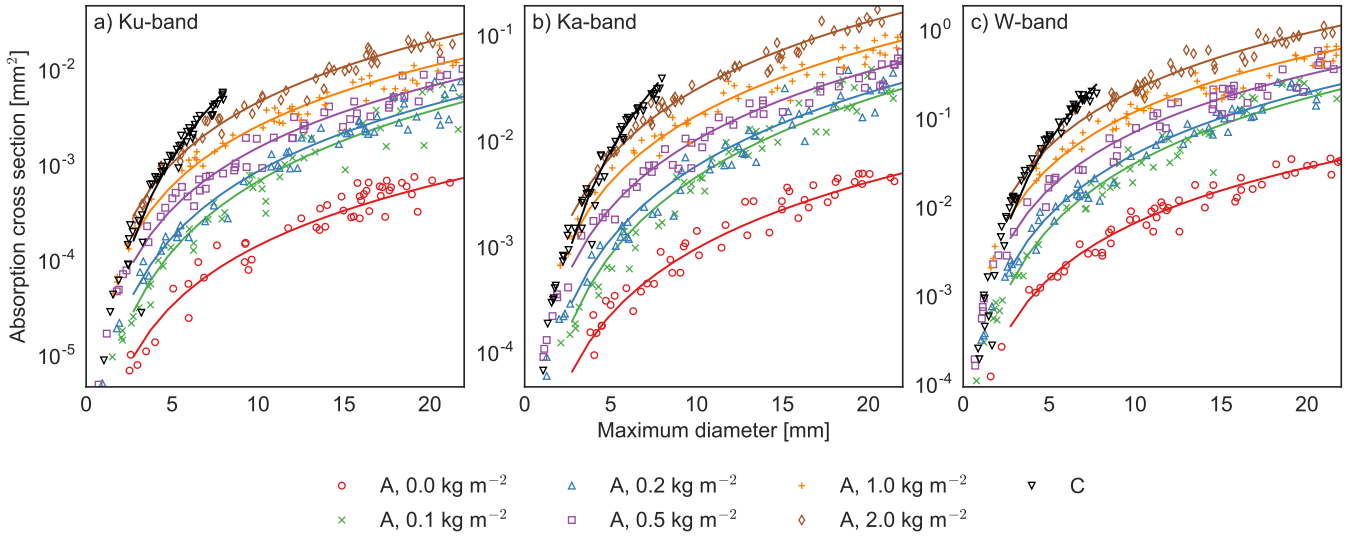

Figure 8. As Fig. 6, but for the absorption cross section C_{abs}.

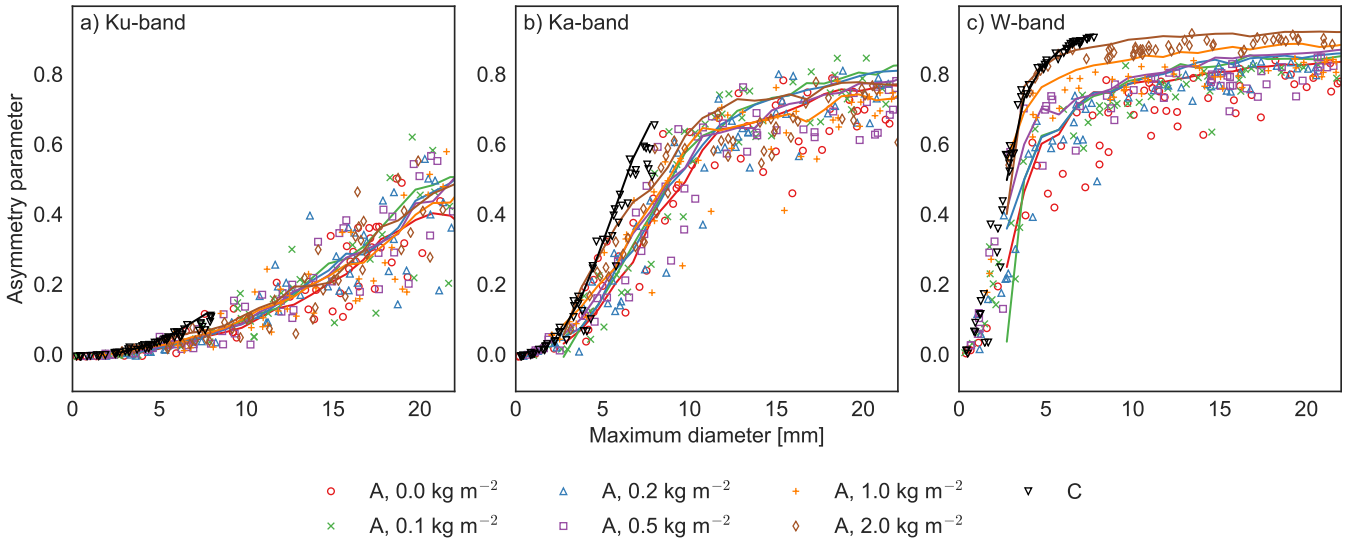

Figure 9. As Fig. 6, but for the asymmetry parameter g.

Hogan RJ, Westbrook CD. 2014. Equation for the microwave backscatter cross section of aggregate snowflakes using the Self-Similar Rayleigh–Gans Approximation. *J. Atmos. Sci.* **71**(9): 3292–3301, doi:10.1175/JAS-D-13-0347.1.

Ishimoto H. 2008. Radar backscattering computations for fractal-shaped snowflakes. *J. Meteor. Soc. Japan* **86**(3): 459–469, doi:10.2151/JMSJ.86.459.

Kneifel S, Kollias P, Battaglia A, Leinonen J, Maahn M, Kalesse H, Tridon F. 2016. First observations of triple-frequency radar Doppler spectra in snowfall: Interpretation and applications. *Geophys. Res. Lett.* **43**(5): 2225–2233, doi:10.1002/2015GL067618.

Kneifel S, von Lerber A, Tiira J, Moisseev D, Kollias P, Leinonen J. 2015. Observed relations between snowfall microphysics and triple-frequency radar measurements. *J. Geophys. Res. Atmos.* **120**: 6034–6055, doi:10.1002/2015JD023156.

Korolev A, Isaac G. 2003. Roundness and aspect ratio of particles in ice clouds. *J. Atmos. Sci.* **60**(15): 1795–1808, doi:10.1175/1520-0469(2003)060<1795:RAAROP>2.0.CO;2.

Kulie MS, Hiley MJ, Bennartz R, Kneifel S, Tanelli S. 2014. Triple frequency radar reflectivity signatures of snow: Observations and comparisons to theoretical ice particle scattering models. *J. Appl. Meteor. Climatol.* : 1080–1098doi:10.1175/JAMC-D-13-066.1.

Leinonen J, Kneifel S, Moisseev D, Tyynelä J, Tanelli S, Nousiainen T. 2012. Evidence of nonspheroidal behavior in millimeter-wavelength radar observations of snowfall. *J. Geophys. Res.* **117**: D18205, doi:10.1029/2012JD017680.

Leinonen J, Moisseev D. 2015. What do triple-frequency radar signatures reveal about aggregate snowflakes? *J. Geophys. Res.* **120**: 229–239, doi:10.1002/2014JD022072.

Leinonen J, Moisseev D, Nousiainen T. 2013. Linking snowflake microstructure to multi-frequency radar observations. *J. Geophys. Res.* **118**, doi:10.1002/jgrd.50163.

Leinonen J, Szyrmer W. 2015. Radar signatures of snowflake riming: A modeling study. *Earth Space Sci.* **2**: 346–358, doi:10.1002/2015EA000102.

Mace G, Benson S. 2017. Diagnosing cloud microphysical process information from remote sensing measurements; a feasibility study using aircraft data. Part I: Tropical anvils measured during TC4. *J. Appl. Meteor. Climatol.* doi:10.1175/JAMC-D-16-0083.1. Early online release available.

Mitchell DL, Zhang R, Pitter RL. 1990. Mass-dimensional relationships for ice particles and the influence of riming on snowfall rates. *J. Appl. Meteor.* **29**(2): 153–163, doi:10.1175/1520-0450(1990)029<0153:MDRFIP>2.0.CO;2.

Mülmenstädt J, Sourdeval O, Delanoë J, Quaas J. 2015. Frequency of occurrence of rain from liquid-, mixed-, and ice-phase clouds derived from A-Train satellite retrievals. *Geophys. Res. Lett.* **42**(15): 6502–6509, doi:10.1002/2015GL064604. 2015GL064604.

Petty GW, Huang W. 2010. Microwave backscatter and extinction by soft ice spheres and complex snow aggregates. *J. Atmos. Sci.* **67**(3): 769–787, doi:10.1175/2009JAS3146.1.

Schmitt CG, Heymsfield AJ. 2010. The dimensional characteristics of ice crystal aggregates from fractal geometry. *J. Atmos. Sci.* **67**(5): 1605–1616, doi:10.1175/2009JAS3187.1.

Seliga TA, Bringi VN. 1976. Potential use of radar differential reflectivity measurements at orthogonal polarizations for measuring precipitation. *J. Appl. Meteor.* **15**(1), doi:10.1175/1520-0450(1976)015<0069:PUORDR>2.0.CO;2.

Sorensen CM. 2001. Light scattering by fractal aggregates: A review. *Aerosol Sci. Technol.* **35**: 648–687, doi:10.1080/02786820117868.

Stein THM, Westbrook CD, Nicol JC. 2015. Fractal geometry of aggregate snowflakes revealed by triple-wavelength radar measurements. *Geophys. Res. Lett.* **43**, doi:10.1002/2014GL062170.

Tyynelä J, Leinonen J, Moisseev D, Nousiainen T. 2011. Radar backscattering from snowflakes: comparison of fractal, aggregate and soft-spheroid models. *J. Atmos. Oceanic Technol.* **28**: 1365–1372, doi:710.1175/JTECH-D-11-00004.1.

Tyynelä J, Leinonen J, Westbrook C, Moisseev D, Nousiainen T. 2013. Applicability of the Rayleigh-Gans approximation for scattering by snowflakes at microwave frequencies in vertical incidence. *J. Geophys. Res.* **118**, doi:10.1002/jgrd.50167.

van de Hulst HC. 1957. *Light scattering by small particles*. John Wiley & Sons: New York, USA.

Warren SG, Brandt RE. 2008. Optical constants of ice from the ultraviolet to the microwave: A revised compilation. *J. Geophys. Res.* **113**(D14), doi: 10.1029/2007JD009744.

Westbrook CD. 2014. Rayleigh scattering by hexagonal ice crystals and the interpretation of dual-polarisation radar measurements. *Quart. J. Roy. Meteor. Soc.* **140**(683): 2090–2096, doi:10.1002/qj.2262.

Westbrook CD, Ball RC, Field PR, Heymsfield AJ. 2004a. Theory of growth by differential sedimentation, with application to snowflake formation. *Phys. Rev. E* **70**(2): 021 403, doi:10.1103/PhysRevE.70.021403.

Westbrook CD, Ball RC, Field PR, Heymsfield AJ. 2004b. Universality in snowflake aggregation. *Geophys. Res. Lett.* **31**(15): L15104, doi: 10.1029/2004GL020363.

Xu Z, Mace GG. 2017. Ice particle mass-dimensional relationship retrieval and uncertainty evaluation using the optimal estimation methodology applied to the MACPEX data. *J. Appl. Meteor. Climatol.* doi:10.1175/JAMC-D-16-0222.1. Early online release available.

Yurkin MA, Hoekstra AG. 2011. The discrete-dipole-approximation code ADDA: Capabilities and known limitations. *J. Quant. Spectrosc. Radiat. Transfer* **112**: 2234–2247, doi:10.1016/j.jqsrt.2011.01.031.

Zubko E, Petrov D, Grynko Y, Shkuratov Y, Okamoto H, Muinonen K, Nousiainen T, Kimura H, Yamamoto T, Videen G. 2010. Validity criteria of the discrete dipole approximation. *Appl. Opt.* **49**(8): 1267–1279, doi: 10.1364/AO.49.001267.

